Available online at www.sciencedirect.com
ScienceDirect
Comput. Methods Appl. Mech. Engrg. 197 (2008) 2329–2339
Computer methods in applied mechanics and engineering
www.elsevier.com/locate/cma

Computational models of valveless pumping using the immersed boundary method

Eunok Jung [a,*], Sookkyung Lim [b,1], Wanho Lee [a], Sunmi Lee [a]

[a] Department of Mathematics, Konkuk University, 1 Hwayang-dong, Gwangjin-gu, Seoul 143-701, Republic of Korea
[b] Mathematical Biosciences Institute, Ohio State University, 231 West 18th Avenue, Columbus, OH 43210, USA

Received 30 December 2007; received in revised form 15 January 2008; accepted 21 January 2008
Available online 10 March 2008

Abstract

Mathematical models of valveless pumping can be represented by either a closed loop system or an open tube system. In this paper, we present a three-dimensional model of valveless pumping in a closed loop system. We also present a two-dimensional model using an open elastic cylinder contained in a rigid tank. In both models, we take the periodic compress-and-release action at the asymmetric location of the soft tube and observe the existence of a net flow and the important features of valveless pumping that have been reported in the previous models or experiments. The innovative idea of this work is that we explain the existence of a net flow by introducing the concept of the signed area of the flow-pressure loop over one cycle, which represents the power in the system. The direction and the magnitude of a net flow can also be explained by the sign and the amount of power, which is work done on the fluid by the fluid pressure and the elastic wall over one period, respectively.

Keywords: Valveless pumping; Immersed boundary method; Circulation; Power; Asymmetric pump

1. Introduction

Mathematical models of valveless pumping can be represented by either a closed loop system or an open system that consists of a couple of tubes with different elasticities or radii. A unidirectional net flow is observed in a valveless pump model when the asymmetric periodic force is applied on the system. We call this phenomenon *valveless pumping*. For decades, both experimental and computational researches on valveless pumping have been intensively studied. Research on valveless pumping was originally motivated to understand the mechanism of the blood circulatory system. There are cases in nature of unidirectional net flow in the circulatory system even with malfunctioning valves. For example, the mechanism of valveless pumping may explain unidirectional blood circulation in the human embryo prior to the end of the third week of gestation, when cardiac valves first are developed [18]. Scientists proposed theories to explain the mechanism of a unidirectional blood flow during cardiopulmonary resuscitation (CPR). One of the main theories is a thoracic pump mechanism, in which blood circulation occurs when some of the valves do not function normally [1–4]. Valveless pumping may explain the underlying mechanism of the thoracic pump. Recently, the physical experiments of a micro-scaled version of valveless pumping in an open or a closed loop system were developed by Hickerson et al. [5,22]. The mechanism of valveless pumping can be applied not only to macrofluid dynamics but also to microfluidics and micro devices.

A physical experiment of valveless pumping in a closed loop model was first suggested by Liebau [9–11]. Liebau presented the mechanism of valveless pumping in the circulation

* Corresponding author. Tel.: +82 2 450 4163; fax: +82 2 458 1952.
E-mail addresses: junge@konkuk.ac.kr (E. Jung), limsk@math.uc.edu (S. Lim), lwh3958@konkuk.ac.kr (W. Lee), sunlee@konkuk.ac.kr (S. Lee).
[1] Present address: Department of Mathematical Sciences, University of Cincinnati, 839 Old Chem, Cincinnati, OH 452221, USA.

0045-7825/$ - see front matter © 2008 Elsevier B.V. All rights reserved.
doi:10.1016/j.cma.2008.01.024

during early embryonic life [9], energy transfer from arterioles to venules [12], and the tissue capillary circulation [13]. Thomann initiated a mathematical model, a one-dimensional model for periodic, inviscid, and incompressible flow [23]. Moser et al. presented a lumped electric model in a closed loop [19]. Jung and Peskin first developed a two-dimensional computational model of valveless pumping in a closed loop [6,7]. They showed the direction and magnitude of a net flow are dependent not only on the position of pumping but also parameters such as frequency of the oscillatory force. Ottesen developed a one-dimensional model of valveless pumping by averaging the Navier–Stokes equations, ignoring higher-order terms in a certain small quantity [20]. Recently, Manopoulous et al. have reported qualitative results from their quasi-one-dimensional model [15]. Jung developed a simple lumped model system governed by the ODE equations with the time-dependent compliances, resistances, and inertia [8].

In this paper, we present two new models of valveless pumping using the immersed boundary method. A three-dimensional model of valveless pumping in a closed loop system is first presented. As mentioned earlier, the various types of the mathematical models of valveless pumping have been developed, for example, lumped models [8,19], one-dimensional models [15,20,23], and two-dimensional models [6,7]. These models have provided qualitative analysis and discovered new mechanisms of valveless pumping. However, the details of fluid motions or the wave motions along the tube can not be investigated in the previous models. The three-dimensional model will allow us to analyze the fluid dynamics in a valveless pump. The movies for the motions of fluid dynamics inside the closed loop are referenced in the following website: http://math.konkuk.ac.kr/~junge/vp3d.html.

Next, we present a two-dimensional model of valveless pumping. The two-dimensional model is composed of an open elastic tube enclosed by a rigid rectangle, and they are separated unlike most other related approaches: *two different materials do not need to be connected in a valveless pump system to generate a net flow*. Although the elastic and the rigid parts are separated, we have observed main features of valveless pumping. A striking result of this work is that we could explain the fundamental question of valveless pumping: why does a net flow exist in a valveless pump system? We introduce the concept of the signed area of a flow-pressure loop over one cycle, which implies the power. With the concept of the net signed area, the direction and magnitude of a net flow can be explained in terms of the sign and the amount of power, which is work done on the fluid by fluid pressure and the elastic wall over one period, respectively. In the two-dimensional and three-dimensional models, we have showed that the direction and magnitude of the net flow are dependent not only upon the position of pumping but also the frequency and the amplitude of the driving function.

In Section 2, we introduce a three-dimensional mathematical model of a closed loop valveless pump system, describe the immersed boundary method, and discuss numerical results. In Section 3, we present a two-dimensional valveless pump model of an open elastic cylinder contained in a closed rigid tank and discuss the numerical results. Summary and conclusion are presented in the final section.

2. A three-dimensional model of a closed loop valveless pump system

Our three-dimensional model is a closed loop that consists of an open rigid tube (rigid straight cylinder) connected by two half tori at both ends of the rigid tube and an open soft tube (elastic straight cylinder). This closed loop is embedded in a cuboid filled with a viscous incompressible fluid. The diameter of each tube is the same so that the two tubes with different materials can be joined smoothly. The length of the soft tube is L, the half of the fluid domain in the y-direction, as shown in Fig. 1. Dimensions and parameters of the computational model are listed in Table 1.

A pumping force is generated by a cosine function in space and time, which will be described in Section 2.1. This force is applied to one third of the soft tube from the left end by way of a periodic compress-and-release action with a time delay between actions. A net flow is created by periodically compressing the soft tube at the asymmetric location. In computations, the closed loop is discretized, and is composed of springs in a way that each material point of the loop is linked to four adjacent material points (see Fig. 2).

2.1. Equations of motion

The immersed boundary (IB) method is both a mathematical formulation and a numerical scheme. There are two types of variables, Eulerian and Lagrangian variables. Eulerian variables are defined on the fixed Cartesian coordinates and used for fluid equations. Lagrangian variables

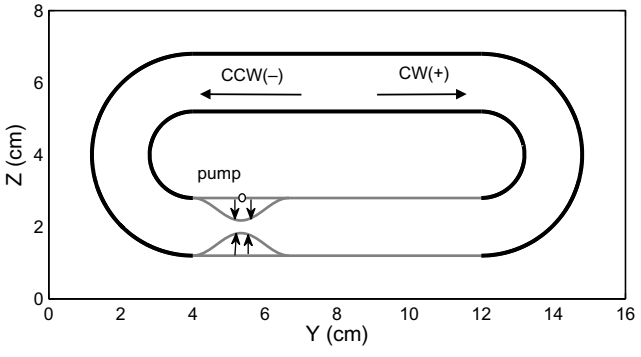

Fig. 1. A cross section in the middle of a three-dimensional model of valveless pump immersed in a viscous fluid. There are two flow directions: counterclockwise (CCW) and clockwise (CW). The closed loop consists of a rigid tube (thick line) and a soft tube (thin line). Periodic pumping force is applied to one third of the soft tube from the left end. Target position of the middle point (○) of the pump is shown in Fig. 3.

Table 1
Parameters for the three-dimensional model (CGS units)

Parameters	Notation	Values
Fluid density	ρ	1 g/cm^3
Fluid viscosity	μ	0.01 g/(cm s)
Computational domain	$L_x \times L_y \times L_z$	4 cm × 16 cm × 8 cm
Duration of experiment	$t_{\max}$	50 s
Stiffness (rigid tube)	c_t	1000 g/(s^2 cm)
Stiffness (soft tube)	c_t	10 g/(s^2 cm)
Stretch stiffness	c_s	100 g cm/s^2
Bending coefficient	c_b	0.2 g cm^3/s^2
Amplitude (target)	a	0.0625 ∼ 0.5 cm
Frequency	f	0.25 ∼ 3 Hz
Compression duration	d	0.5
Meshwidth	$h = \Delta x = \Delta y = \Delta z$	0.125 cm
Time step	Δt	0.001 s
Diameter of tube		1.6 cm
Fluid grid		32 × 128 × 64

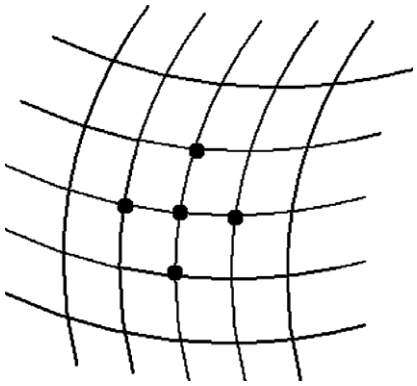

Fig. 2. Each material point of the closed tube is connected to four adjacent points.

are defined on the curvilinear coordinates that move through the fluid and used for the structure equations in which the closed tube is immersed in the fluid. These two different forms are communicating one another via the Dirac delta function δ.

A coupled system of equations that describe the fluid-tube interaction is formulated as follows:

$$\rho\left(\frac{\partial \mathbf{u}}{\partial t} + \mathbf{u}\cdot\nabla\mathbf{u}\right) = -\nabla p + \mu\nabla^2\mathbf{u} + \mathbf{f}, \tag{1}$$

$$\nabla\cdot\mathbf{u} = 0, \tag{2}$$

$$\mathbf{f}(\mathbf{x},t) = \int \mathbf{F}(r,s,t)\delta(\mathbf{x}-\mathbf{X}(r,s,t))\,\mathrm{d}r\,\mathrm{d}s, \tag{3}$$

$$\frac{\partial \mathbf{X}(r,s,t)}{\partial t} = \mathbf{u}(\mathbf{X}(r,s,t)) = \int \mathbf{u}(\mathbf{x},t)\delta(\mathbf{x}-\mathbf{X}(r,s,t))\,\mathrm{d}\mathbf{x}, \tag{4}$$

$$\mathbf{F}(r,s,t) = c_t(\mathbf{Z}(r,s,t)-\mathbf{X}(r,s,t)) - \frac{\partial E}{\partial \mathbf{X}}, \tag{5}$$

$$E[\mathbf{X}(r,s,t)] = \frac{1}{2}c_s\int\left(\left|\frac{\partial \mathbf{X}}{\partial s}\right|-1\right)^2\mathrm{d}s + \frac{1}{2}c_b\int\left|\frac{\partial^2\mathbf{X}}{\partial s^2}\right|^2\mathrm{d}s. \tag{6}$$

The fluid Eqs. (1) and (2) are the viscous incompressible Navier–Stokes equations in Eulerian form. They involve several unknown functions of $(\mathbf{x},t)$, where $\mathbf{x}=(x,y,z)$ are fixed Cartesian coordinates and t is time. The unknown functions are fluid velocity $\mathbf{u}(\mathbf{x},t)$, fluid pressure $p(\mathbf{x},t)$, and the force density $\mathbf{f}(\mathbf{x},t)$ applied by the immersed boundary to the fluid. The constant parameters ρ and μ are the fluid density and viscosity, respectively.

Eqs. (3) and (4) are the interaction equations between the fluid and the immersed boundary. Both equations involve the three-dimensional Dirac δ-function. Eq. (3) describes the relationship between the fluid force density $\mathbf{f}(\mathbf{x},t)$ and the boundary force density $\mathbf{F}(r,s,t)$. Eq. (4) is the no-slip condition of the viscous fluid, which restricts the immersed boundary to move at the local fluid velocity. Each of the interaction equations takes the form of an integral transformation in which the kernel is $\delta(\mathbf{x}-\mathbf{X}(r,s,t))$.

Finally, Eq. (5) is the immersed boundary equation in Lagrangian form. The variable $\mathbf{X}(r,s,t)$ describes the motion of the immersed boundary and its configuration at any time, where (r,s) are moving curvilinear coordinates. Here, r is a designated fiber and s is arc length along the fiber. $\mathbf{Z}(r,s,t)$ is the *target position* of the immersed boundary. The formulation of the target position will be described in detail later. The energy function E in the second term in Eq. (5) is the elastic energy from stretching and bending, and is described in Eq. (6) where c_s is stiffness for the elastic boundary and c_b is bending coefficient. Although the tethering force, the first term in Eq. (5), is sufficient to fix the rigid tube, we applied the stretching and bending forces to the rigid part also because the soft and rigid tubes are connected. In this way, there is no need to add any special condition in order to calculate stretching and bending forces at the connection part. We used the same stretch stiffness (c_s) and bending coefficient (c_b) for the whole closed loop. However, two different values of stiffness (c_t) are used for the target position, see Table 1. Note that $\mathbf{X}(r,s,t)$ is a two-dimensional surface in a three-dimensional space, and the closed loop is represented by a mesh of fibers. Therefore, the total elastic energy is the summation of the internal energies within individual fibers.

The variational derivative $\frac{\partial E}{\partial \mathbf{X}}$ of the energy functional $E[]$ is defined as follows:

$$\lim_{\epsilon\to 0}\frac{\mathrm{d}}{\mathrm{d}\epsilon}E[\mathbf{X}+\epsilon\mathbf{Y}] = \int\frac{\partial E}{\partial \mathbf{X}}(r,s,t)\cdot\mathbf{Y}(r,s,t)\,\mathrm{d}r\,\mathrm{d}s \tag{7}$$

and hence the elastic force derived from the Eq. (6) is induced by

$$-\frac{\partial E}{\partial \mathbf{X}} = \frac{\partial}{\partial s}(T\boldsymbol{\tau}) + c_b\frac{\partial^4\mathbf{X}}{\partial s^4}, \tag{8}$$

where

$$T = c_s\left(\left|\frac{\partial \mathbf{X}}{\partial s}\right|-1\right), \tag{9}$$

$$\boldsymbol{\tau} = \frac{\frac{\partial \mathbf{X}}{\partial s}}{\left|\frac{\partial \mathbf{X}}{\partial s}\right|}. \tag{10}$$

Here, T is the tension derived from Hook's law and $\boldsymbol{\tau}$ is the unit tangent vector. Note that we chose the initial configuration as the equilibrium configuration.

Now we describe the mathematical formulation of the target position $\mathbf{Z}(r,s,t)$. The target position plays two roles: a time-dependent part as a periodic pumping source and a time-independent part for maintaining the shape of the flow loop. In most cases of our simulations, the time-dependent target position is applied on the left third of the flexible tube of the flow loop, with the time-independent target position being the rest of the flow loop. Let $\mathbf{X}(r,s,0) = (x_0(r,s,0), y_0(r,s,0), z_0(r,s,0))$ be the initial position of the elastic boundary and $\mathbf{Z}(r,s,t) = (x_p(r,s,t), y_p(r,s,t), z_p(r,s,t))$ be the target position at any time t, where (r,s) is restricted to the left third of the flexible tube. Note that this part will be working as a pumping source.

We define a driving force using a cosine function with one period in space and time as follows:

$$A(r,s,t) = \begin{cases} -\frac{a}{4}\left(\cos\left(\frac{2\pi}{\mathrm{d}\mathscr{P}}t\right) - 1\right)\left(\cos\left(2\pi\frac{y_0(r,s,0)-0.25L_y}{\frac{1}{3}L}\right) - 1\right) \\ \text{if } 0 \leqslant \mathrm{mod}\ (t,\mathscr{P}) \leqslant \mathrm{d}\mathscr{P}, \\ 0 \\ \text{if } \mathrm{d}\mathscr{P} \leqslant \mathrm{mod}(t,\mathscr{P}) \leqslant \mathscr{P}, \end{cases} \tag{11}$$

$$B(r,s,t) = z_0(r,s,0) - 0.25L_z, \tag{12}$$

where a is the amplitude of the pump and $\mathscr{P}$ denotes the period, i.e., $f = \frac{1}{\mathscr{P}}$ is the frequency of oscillations. $\mathrm{d}\mathscr{P}$ is the duration of compression, where $0 \leqslant d \leqslant 1$, and the function $A(r,s,t)$ remains constant for the time $(\mathscr{P} - \mathrm{d}\mathscr{P})$ of the period. L_α is the length of the computational domain $[0,L_x] \times [0,L_y] \times [0,L_z]$ in each direction, where $\alpha = x,y,z$ and again this pump is only working on the left third of the flexible tube, $\frac{1}{3}L = \frac{1}{6}L_y$. The three components of the time-dependent target position are described by

$$x_p(r,s,t) = A(r,s,t)\cos\theta - B(r,s,t)\sin\theta + 0.5L_x, \tag{13}$$

$$z_p(r,s,t) = A(r,s,t)\sin\theta - B(r,s,t)\cos\theta + 0.25L_z, \tag{14}$$

$$y_p(r,s,t) = y_0(r,s,0), \tag{15}$$

where $0 \leqslant \theta < 2\pi$.

Fig. 3 shows the target position of the middle point of the pumping part during one period. Four different values of d, 1, 1/2, 1/3, and 1/4, were considered and displayed from the top panel to the bottom one, respectively. Thus, the target position of the pump follows the Eqs. (13)–(15), and that of the rest of the closed loop is set to be the initial configuration.

We employ the numerical scheme that has been described in [14,21,24] with concrete explanation. The fluid equations in Eulerian variables are discretized on a fixed Cartesian mesh and the boundary equations in Lagrangian variables are discretized on a moving curvilinear mesh. These two types of variables are linked by interaction equations that involve a smoothed approximation to the Dirac delta function. We assume that the fluid domain is periodic.

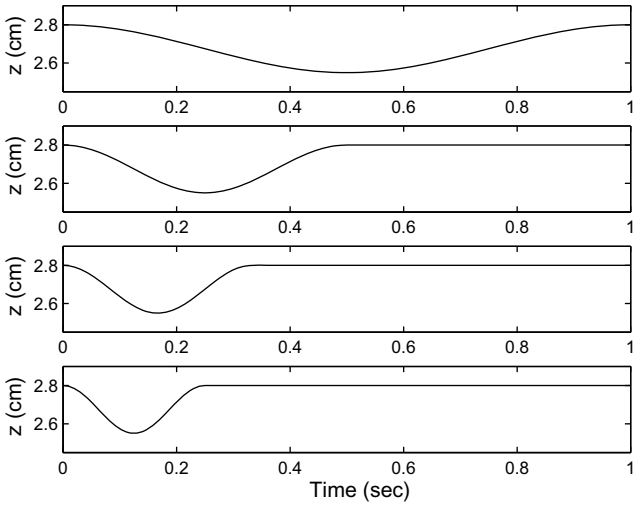

Fig. 3. Target position of the middle point of the pumping part over one cycle (see the position of the middle point (○) in Fig. 1). Parameter value of the compression duration is $d = 1$ for the top panel, $d = \frac{1}{2}$ for the second panel, $d = \frac{1}{3}$ for the third panel, and $d = \frac{1}{4}$ for the bottom panel.

2.2. Numerical results and discussion

Average flow was measured on the cross section in the middle of the top rigid cylinder. The simulated time is 50 s for each computational experiment. This is after the flow rate becomes steady. Fig. 4 shows three examples of typical responses of average flow in time. The parameter values are chosen for (a) $f = 3$ Hz, $a = 0.375$ cm, (b) $f = 3$ Hz, $a = 0.1875$ cm, and (c) $f = 0.25$ Hz, $a = 0.4375$ cm. The sign of the average flow indicates the direction of the flow inside the tube, positive values for clockwise (CW) and negative values for counterclockwise (CCW) direction. These examples show that the direction of the

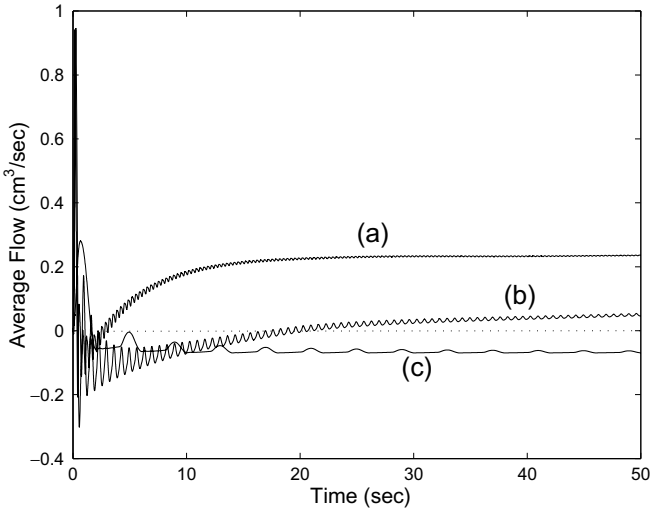

Fig. 4. Examples of typical average flow change in time. The direction of the flow is either clockwise (positive value), or counterclockwise (negative value). The parameter values are (a) $f = 3$ Hz, $a = 0.375$ cm, (b) $f = 3$ Hz, $a = 0.1875$ cm, and (c) $f = 0.25$ Hz, $a = 0.4375$ cm.

flow is CW for case (a) and CCW for case (c) after the steady-state is reached. Case (b) illustrates the change of the sign around $t = 20$ s, which indicates flow reversal, and eventually shows CW flow direction.

The volume of the closed loop can be evaluated by integrating by means of the Divergence theorem. The theorem states that: given a region V and its surface S

$$\int\int\int_V \nabla \cdot \mathbf{G}\,\mathrm{d}V = \int\int_S \mathbf{G} \cdot \mathbf{n}\,\mathrm{d}S, \tag{16}$$

where $\mathbf{G}$ is a vector function with continuous partial derivatives, $\mathbf{n}$ is the unit vector normal to the surface.

With a discretized model we can approximate the volume of the closed loop by triangulating the surface of the loop [16,17]. It is important to keep the orientation of each triangle the same in volume calculations, i.e., the vertices of each triangle proceed counterclockwise when viewed from the outside of the closed loop. According to the right-hand rule, this causes a normal vector of the triangle facet to point outward. Note that the surface of our model is the moving boundary as time progresses, and it gives less accurate volume than that of the solids. In these simulations, the change of the volume remains within 13%.

The average flow as a function of time is measured when the driving function is applied on the three different locations: left third, middle third, and right third of the soft tube. All parameters for these experiments are fixed except for the pumping location. Periodic oscillatory motions are observed, that is, flow pattern of each period appears to be same within each simulation. The magnitude of the oscillatory motions for the case of left third and right third converges to 1.2 cm^3/s and -1.2 cm^3/s, respectively. This is an expected result because of the symmetry of the closed loop system. This phenomenon has also been observed in physical experiments [5,9–11,20,22]. As expected, almost zero net flow is observed over the simulated time when the middle part of the soft tube is chosen for the pumping source. This indicates that an asymmetric driving force is required to generate a net flow of valveless pumping.

We observe the effect of the pumping frequency and amplitude of the oscillations on the average flow. Fig. 5 shows the average flow as a function of the pumping frequency, f, for various values of amplitude, a. The amplitude ranges from 0.0625 cm to 0.5 cm and the frequency from 0.25 Hz to 3 Hz. While keeping the amplitude same, the direction of the net flow changes due to a change in pumping frequency. Similarly, when we fix the pumping frequency, changes in amplitude switch the direction of the net flow. For low amplitudes the direction of the net flow is CCW for low frequencies, however, the net flow tends to be in the opposite direction for frequencies above 2.5 Hz. For higher amplitudes the change of the flow direction occurs at the small frequencies from CCW to CW. The magnitude of net flow reaches maximum value around the frequency of 2 Hz with high amplitudes. In general, we observe small magnitude for lower amplitudes and large magnitude for higher amplitudes. Flow reversal occurs at

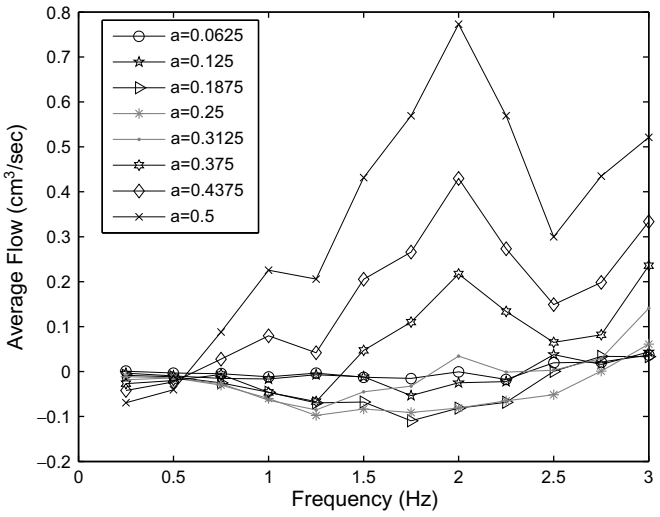

Fig. 5. Average flow versus frequency. a is the amplitude of the target position of the pump in centimeters.

the frequencies where the direction of net flow changes from CCW to CW, for example, at the frequency $f = 0.75$ Hz with the amplitude $a = 0.4375$ cm, $f = 1.5$ Hz with $a = 0.375$ cm, and $f = 2$ Hz with $a = 0.3125$ cm.

3. A two-dimensional valveless pump model of an open elastic cylinder contained in a rigid tank

In this section, we introduce a two-dimensional model of a valveless pump system. The model is represented by two different materials: one is an open elastic cylinder located at the center of the fluid domain and the other is a closed rigid tank which encompasses the open cylinder. Although the two materials are not connected each other (see Fig. 6), we could observe the important characteristics of valveless pumping as the earlier computational models or the experiments showed.

3.1. Equations of motion

We consider a viscous incompressible fluid which fills a periodic rectangular box containing a closed (almost) rigid tank and an elastic open tube. Fig. 6 displays the initial configuration of our two-dimensional model. In this two-dimensional model, the immersed boundary consists of one rectangular rigid tank and one elastic open tube (two lines inside the tank). The fluid fills the entire computational box, however, fluid markers are shown only inside the rigid tank because that is the region of interest. The fluid motions are driven by periodic vertical oscillations of the left second quarter of the elastic tube (the pumping location is marked with the upper and lower arrows) in most of our simulations.

We shall now describe the mathematical formulation of the model. The fluid-structure interaction equations are almost the same as the Eqs. (1)–(6). There are minor

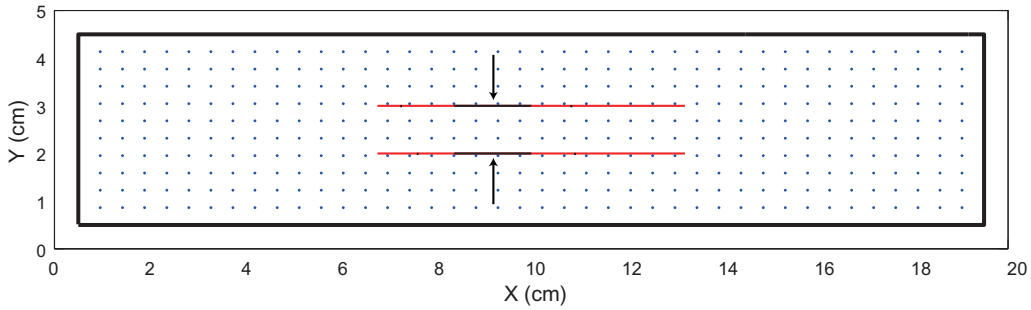

Fig. 6. Initial configuration: Outer rectangular box represents a computational domain. A closed rigid tank (thick line, inner rectangular box), an open elastic tube (thin lines in red), and fluid markers (dots) are displayed. The periodic pumping is applied to the left second quarter of the elastic tube (arrows).

differences. First is the difference in dimension: we use the two-dimensional space in this model. The fluid variable $\mathbf{x}$ now becomes $\mathbf{x} = (x, y)$ and the moving curvilinear coordinate s. The immersed boundary and its target position are denoted by $\mathbf{X}(s,t)$ and $\mathbf{Z}(s,t)$, respectively. Second is the difference in the target position: the time-dependent target position is applied on the left second quarter of the elastic tube; the target position of the rest of the elastic tube is time-independent and is set to be the initial configuration. Let $\mathbf{Z}(s,t) = (Z_x(s), Z_y(s,t))$ be the time-dependent target position, where s is restricted to the range of values that defines the second left quarter of the tube. Note that the x-component of the target position is independent of time t, whereas the y-component varies with time in the manner that we prescribe below.

The driving oscillatory function with one period in space and time is defined as follows:

$$A(s,t) = \begin{cases} a \sin\left(\pi \frac{Z_x(s) - \frac{5}{12}X_{\text{scale}}}{\frac{1}{12}X_{\text{scale}}}\right) \sin\left(\frac{\pi t}{\mathrm{d}\mathscr{P}}\right) \\ \text{if } 0 \leqslant \mathrm{mod}(t, \mathscr{P}) \leqslant \mathrm{d}\mathscr{P}, \\ 0 \\ \text{if } \mathrm{d}\mathscr{P} \leqslant \mathrm{mod}(t, \mathscr{P}) \leqslant \mathscr{P}, \end{cases} \tag{17}$$

where a, d, and $\mathscr{P}$ are the amplitude, the compression duration, and the period of the target position, respectively, and X_{scale} is the length of the computational domain in the x-direction.

The elastic tube begins at $x = \frac{1}{3}X_{\text{scale}}$ and ends at $x = \frac{2}{3}X_{\text{scale}}$. Thus, the length of the whole tube is $\frac{1}{3}X_{\text{scale}}$ and the length of the pumping part is $\frac{1}{12}X_{\text{scale}}$. With $A(s,t)$ defined as above, $Z_y(s,t)$ is defined as follows:

$$Z_y(s,t) = \begin{cases} 0.5Y_{\text{scale}} + r - A(s,t) \\ \text{if } s \text{ lies in the upper segment of the tube,} \\ 0.5Y_{\text{scale}} - r + A(s,t) \\ \text{if } s \text{ lies in the lower segment of the tube,} \end{cases}$$

where r is the resting radius of the tube and Y_{scale} is the length of the computational domain in the y-direction.

Finally, the elastic energy from bending is not taken into account in the two-dimensional model. Thus the elastic energy function E in Eq. (6) is replaced by

$$E[\mathbf{X}(s,t)] = \frac{1}{2}c_{\text{s}} \int \left(\left| \frac{\partial \mathbf{X}}{\partial s} \right| - 1 \right)^2 \mathrm{d}s. \tag{18}$$

The numerical and physical parameters for the two-dimensional model are displayed in Table 2.

3.2. Numerical results and discussion

In this subsection, we present numerical results from the two-dimensional model of an open cylinder enclosed by a rigid box. The main results are as follows. Firstly, a net flow inside the elastic tube is produced by the periodic asymmetric pumping, despite the soft and rigid parts are separated. Secondly, the direction and magnitude of a net flow are sensitively dependent on the pumping frequency. We focus on the crucial factor, frequency, in this paper, although it has been reported in many earlier works that the direction and magnitude are determined not only by the frequency but also many other parameters such as the amplitude and the compression duration of the driving

Table 2
Parameters for the two-dimensional model (CGS units)

Parameters	Notation	Values
Computational domain	$X_{\text{scale}} \times Y_{\text{scale}}$	20 cm × 5 cm
Length of the tube	L	6.67 cm
Radius of the tube	r	0.5 cm
Fluid density	ρ	1 g/cm^3
Fluid viscosity	μ	0.01 g/(cm s)
Frequency	f	0.05 Hz ∼ 10 Hz
Compression duration	d	0.5
Amplitude	a	0.5 cm
Stiffness constant (rigid tank)	c_{t}	26000 g/(s^2 cm)
Stiffness constant (flexible tube)	c_{t}	900 g/(s^2 cm)
Stiffness constant	c_{s}	120 g cm/s^2
Fluid lattice	$N_x \times N_y$	512 × 128
Number of boundary points (flexible tube)	M_1	1366
Number of boundary points (rigid tank)	M_2	4704
Mesh width	$h = \Delta x = \Delta y$	0.039 cm
Initial distance between boundary points	Δs	$h/4 = 0.0156$ cm
Time step	Δt	0.00195 s
Simulated time	$t_{\max}$	50 s

function, the radius and wall thickness of the tube, and the ratio of length of pumping part and the rest of the tube. Lastly, we employ a new concept in order to interpret the existence of a net flow: the direction and the magnitude of a net flow in a valveless pump will be explained by the signed areas of the flow-pressure loops along the tube over one cycle.

3.2.1. Parametric study

We investigate the impact of the pumping frequency on our valveless pump model. Fig. 7 displays the space- and time-averaged flow as a function of the pumping frequency, evaluated at the right end cross section of the elastic tube, $x = 13.33$ cm. The frequency ranges from 0.05 Hz to 10 Hz in which 140 different values are considered. The other parameters are given in Table 2. Each point indicates an individual numerical experiment during the simulated time, 50 s. Positive values denote net flows from left to right, and negative values denote net flows in the opposite direction. The space- and time-averaged flow is defined by the mean flux computed on a cross section of the elastic tube over the simulated time. It is obvious to see in Fig. 7 that valveless pumping has a strong dependence on the pumping frequency as we observed in the previous studies. There seems to be preference for positive net flow. However, the largest amount of net flows is observed in the case of the negative net flow at the frequency $f = 2.15$ Hz. There are several turning points, which imply that at certain frequencies the direction of a net flow is changed. Almost zero net flows can be obtained at these turning frequencies. It is clear to see in Fig. 7 that a net flow seems to disappear at the extremes of the frequencies.

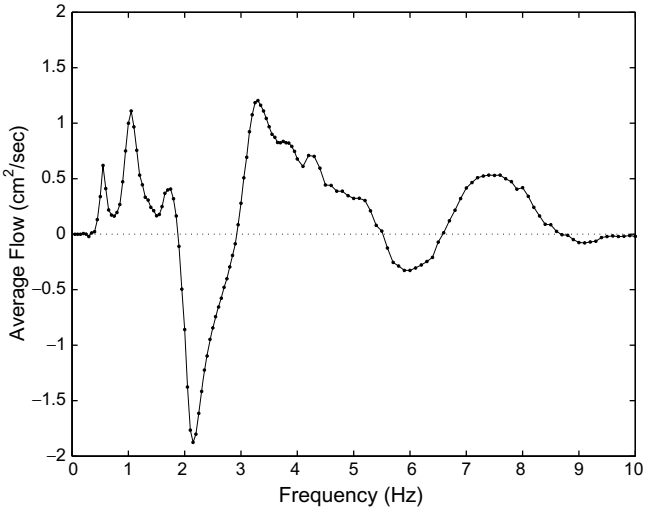

Fig. 7. The space- and time-averaged flows as a function of the frequency are displayed. Net flows are calculated on the right end cross section of the elastic tube, $x = 13.33$ cm. The parameters are given in Table 2 and the compression duration, $d = 0.5$, is chosen. The simulated time of each experiment is 50 s. Positive values denote net flows from left to right and negative values denote net flows in the opposite direction. This figure shows that the frequency is a crucial factor to determine the direction and magnitude of a net flow inside the elastic tube.

3.2.2. Case studies

Three special cases of valveless pumping are studied. We chose the special cases based on the results from the Fig. 7. The maximum positive net flow, an almost zero net flow, and the maximum negative net flow are considered. The space- and time-averaged flows and frequencies for the three cases are given as follows:

- $f = 1.05$ Hz (Positive net flow: 1.1087 cm^2/s)
- $f = 2.95$ Hz (Almost zero net flow: 0.08523 cm^2/s)
- $f = 2.15$ Hz (Negative net flow: -1.8751 cm^2/s)

Recall that the fluid motions are driven by the periodic oscillations imposed on the left second quarter of the elastic tube and a net flow is calculated on the right end cross section of the elastic tube after the steady flow motions. These three cases have been investigated and compared qualitatively in flowmeters and the flow-pressure loops: flowmeters as a function of time are measured to show that the fluid motion becomes periodically steady-state after some time, and to show the nature of the oscillation and the net progress of the fluid motions. In the study of the flow-pressure loops over one period, we introduce a concept of the signed area of a flow-pressure loop and answer the fundamental question in valveless pumping system: *why does a net flow exist in a valveless pump system?*

3.2.2.1. Flowmeter. Fig. 8 displays flowmeters, the average flow computed on the right end cross section of the elastic tube. Flowmeters for positive ($f = 1.05$ Hz), almost zero ($f = 2.95$ Hz), and negative ($f = 2.15$ Hz) net flow cases are plotted in the top, middle, and bottom rows, respectively. Three figures on the left hand side present the space- and time-averaged flows as functions of time during the simulated time, $t = 50$ s, and three figures on the right hand side show the motions of the space-averaged flows as functions of time over the last 5 cycles. As seen in figures on the left column, the motions of the flows are oscillatory and the oscillations have been settled down to the periodic steady motions after the transition period. The case with a low frequency needs longer transition time to get to the steady-state. In the top and bottom figures of the right column, the integral of curves over one cycle takes the positive value in the top figure and negative value in the bottom figure. This shows the existence of a unidirectional net flow in this valveless pump model. As reported in the previous work [7], we have also observed resonances at specific frequencies, which drive the flow most effectively in one direction or the other.

3.2.2.2. The flow-pressure loop. In Fig. 9, the flow-pressure loops over one cycle are displayed after the periodic steady-state is reached. We chose five cross sections along the elastic tube: $x = 6.77$ cm, $x = 8.37$ cm, $x = 10.00$ cm, $x = 11.62$ cm, and $x = 13.23$ cm. The averaged flow (Q) and the averaged pressure (P) are evaluated along the y-direction on the chosen cross sections over one cycle. Top row

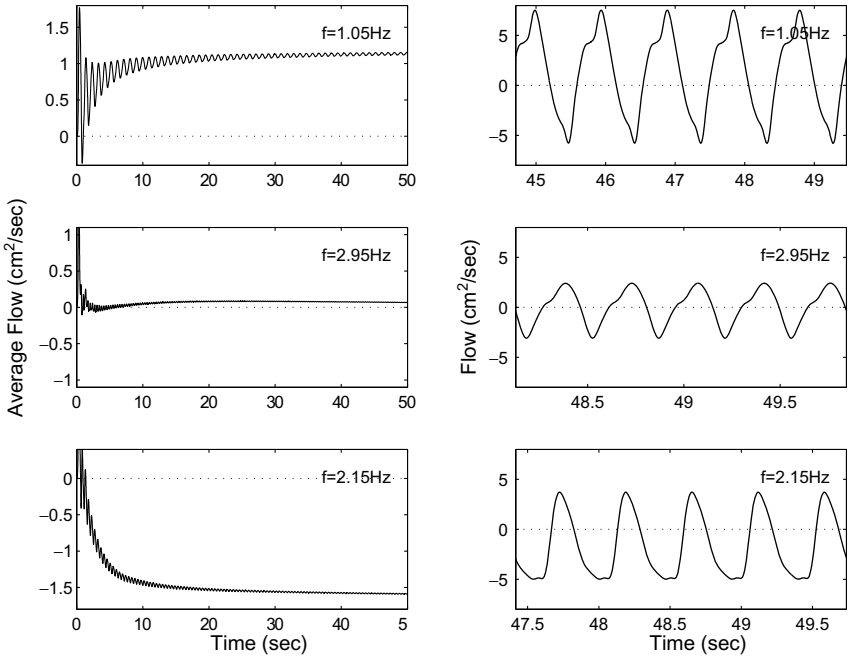

Fig. 8. Flowmeters for positive ($f = 1.05$ Hz), almost zero ($f = 2.95$ Hz), and negative ($f = 2.15$ Hz) net flow cases are plotted in the top, middle, and bottom rows, respectively. Three figures on the left present the space- and time-averaged flows as a function of time during the simulated time, $t = 50$ s, and three figures on the right show the details of the space-averaged flow motions as a function of time over the last 5 cycles.

in Fig. 9 corresponds to the case of positive net flow ($f = 1.05$ Hz), middle row the case of almost zero net flow ($f = 2.95$ Hz), and bottom row the case of negative net flow ($f = 2.15$ Hz). In each row, five flow-pressure loops evaluated on the five cross sections are drawn. In each flow-pressure loop, the red color (the right hand side of a dotted line) and the blue color (the left hand side of a dotted line) are used for positive and negative flows, respectively. An arrow represents the starting point with the direction over one cycle.

We see at a glance in the top row in Fig. 9 that the sum of the areas of the regions surrounded by the red color

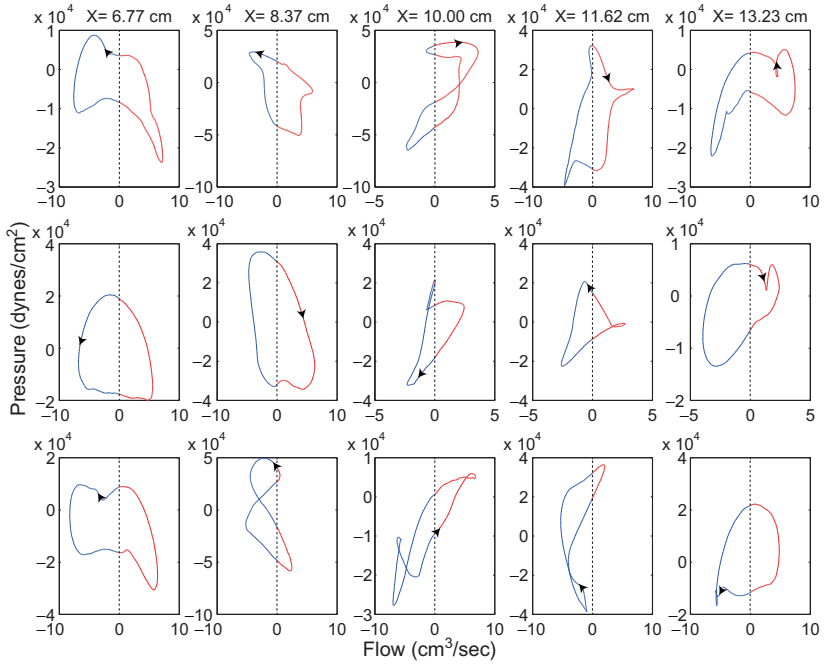

Fig. 9. The flow-pressure loops over one cycle at positive ($f = 1.05$ Hz), almost zero ($f = 2.95$ Hz), and negative ($f = 2.15$ Hz) net flow cases are displayed in the top, middle, and bottom rows, respectively.

(positive flows) is greater than the sum of the areas of the regions surrounded by the blue color (negative flows). Similarly, the sum of the areas surrounded by the red and blue colored curves is almost zero for the middle row, and the sum of the blue colored areas is greater than the sum of the red colored areas for the bottom row. This motivates us to compute the area inside a flow-pressure loop to study the relationship between the area and the direction of a net flow. Since we are interested in the steady-state motions of our system, we consider one period, $T = t_2 - t_1$, after the steady-state is reached. As we anticipated from the physical dimension of the area inside a flow-pressure loop, it represents the power. The area inside a flow-pressure loop can be calculated as follows: $\int_\gamma Q\,dP$, where Q and P represents the flow and pressure, respectively and γ is a closed curve along a flow-pressure loop.

Now we define the signed area, A_{signed}, inside a flow-pressure loop as the difference of two areas, one with the positive flow along the curve $\gamma_+ \cup \gamma_+^0$ and the other with the negative flow along the curve $\gamma_- \cup \gamma_-^0$ (see Fig. 10):

$$A_{\text{signed}} = \int_\gamma |Q|\,dP = \int_{\gamma_+ \cup \gamma_+^0} Q\,dP + \int_{\gamma_- \cup \gamma_-^0} -Q\,dP = A_+ - A_-, \tag{19}$$

where A_+ is the area of the region enclosed by the curve $\gamma_+ \cup \gamma_+^0$ and A_- is the area of the region enclosed by $\gamma_- \cup \gamma_-^0$.

We shall investigate the relationship between the direction of a net flow and the sign of a signed area. We consider the positive flow case ($f = 1.05$ Hz) and the negative flow case ($f = 2.15$ Hz). The space-averaged signed area along the tube is defined as $\mathscr{A} = \frac{1}{N}\sum_{i=1}^{N} A_{\text{signed},i}$, where N is the number of cross sections and $A_{\text{signed},i}$ is the signed area of the ith cross section along the tube. Note that we chose over 500 cross sections along the tube for our simulations. The space-averaged signed areas along the tube and the net flows for the maximum positive and negative flow cases are given in Table 3. This shows that the sign of the net signed area coincides with the sign of the directional net flow. The case of positive net flow at $f = 1.05$ Hz gives the positive net signed area 56,068. On the other hand, the case of negative net flow at $f = 2.15$ Hz gives the negative net signed area −88,387. With this in mind, we present a new approach in a valveless pump system that *the direction of a net flow can be explained by the sign of the power inside the whole tube*.

Table 3
The net flows and the net signed areas

Frequency	Net flow	Net signed area
$f = 1.05$ Hz (positive case)	1.0087	56,068
$f = 2.15$ Hz (negative case)	−1.8751	−88,387

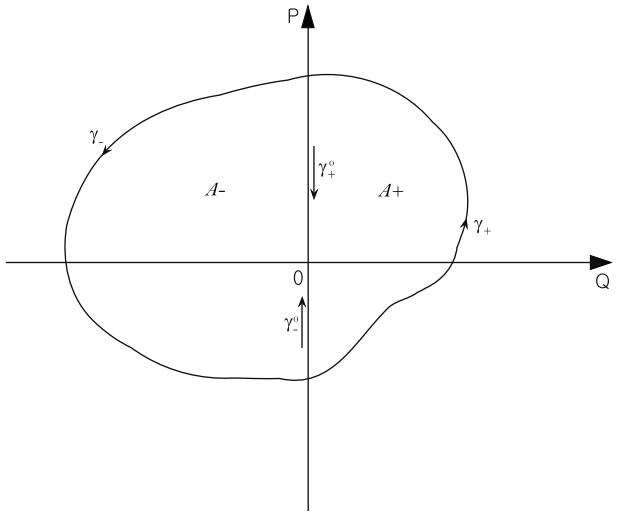

Fig. 10. A flow-pressure loop: the signed area inside a flow-pressure loop, $\gamma = \gamma_+ \cup \gamma_-$ is negative in this case.

The signed area in Eq. (19) can be rewritten in the following way. Let's first consider the curve γ_+, a part of the closed loop (see Fig. 10), and calculate the power along this curve γ_+:

$$\begin{aligned}\int_{\gamma_+} Q\,dP &= \int_{\gamma_+} Av\,dP = \int_{t_1}^{t^*} A(t)v(t)P'(t)\,dt \\ &= \int_{t_1}^{t^*} (A(t)P(t))'v(t)\,dt - \int_{t_1}^{t^*} A'(t)v(t)P(t)\,dt \\ &= \int_{t_1}^{t^*} F'(t)v(t)\,dt - \int_{t_1}^{t^*} A'(t)v(t)P(t)\,dt \\ &= \int_{\gamma_+} v\,dF - \int_{\gamma_+} vP\,dA,\end{aligned} \tag{20}$$

where A is the area of the cross section as a function of time, v and F are the time-dependent averaged velocity and averaged force on the same cross section, respectively, and t^* is time between t_1 and t_2.

Similarly we can rewrite the signed area along the closed curve γ:

$$A_{\text{signed}} = \int_\gamma |Q|\,dP = \int_\gamma |v|\,dF - \int_\gamma |v|P\,dA. \tag{21}$$

On the right hand side of Eq. (21), the first term means the power over one period induced from the fluid pressure, while the second one is the power due to the variation of the elastic wall, i.e., it can be viewed as the elastic power over one period. Therefore, the signed area becomes the sum of the pressure-induced power and the elastic power over one period.

Now we can define a net signed area along the tube by net power along the tube over one period. Note that in Table 3 the bigger magnitude of a net flow corresponds to the bigger net signed area. This result shows that *the larger net flow can be induced by the larger net power, which is work done on the fluid by fluid pressure and the elastic wall over one period*.

In this work, we show two important features of a valveless pump system from the signed area inside a flow-pressure loop. The sign of a directional net flow has the same

sign of the signed area, which implies that the direction of a net flow can be explained by the sign of power. The bigger net flow has the bigger magnitude of the signed area, which implies that the magnitude of a net flow can be explained by the amount of net power over one cycle, that is the rate of energy change along the tube over one period.

4. Summary and conclusion

We have presented two mathematical models of flows driven by pumping without valves, valveless pumping, using the immersed boundary method: one is a three-dimensional model of a closed loop system and the other is a two-dimensional model of a closed rigid tank which encompasses an open elastic cylinder. There have been intensive studies on the valveless pump system for decades. In particular, lumped models, one-dimensional models, and two-dimensional models have been developed to explain the valveless pump mechanism. Due to dimensional reduction, however, the fluid dynamics occurred in a three-dimensional space can not be observed in the previous models. This led us to propose a three-dimensional model of a valveless pump.

In earlier models and physical experiments of valveless pumping, two different elasticities or radii of tubes have been used in either a closed loop system or an open system of valveless pumping, in which the tubes with different material or geometrical properties are joined smoothly. In this paper, we have developed a model of valveless pumping using two different materials which are not connected to each other. A closed (almost) rigid tank containing an open elastic straight tube is used in the two-dimensional model.

In both proposed models, we have observed the existence of net flows: *valveless pumping*. In simulations of the three-dimensional closed loop model, we have investigated that the direction and magnitude of the net flow are determined sensitively by the frequency and the amplitude of the driving oscillations. For the fluid dynamics the movies of the simulations can be viewed at the website: http://math.konkuk.ac.kr/∼junge/vp3d.html.

In the study of the two-dimensional model of an open elastic cylinder enclosed by a rigid tank, we have observed the following results in the model: the pumping frequency is the crucial factor to decide the direction and the magnitude of a net flow. We have studied three special cases for positive, almost zero, and negative net flows. Flowmeters and the flow-pressure loops in each case have been studied. In all cases, the oscillatory steady flows are observed after the transition time. The resonances at peak frequencies are observed. We have shown new features of a valveless pump system by introducing the signed area of a flow-pressure loop: the sign of a directional net flow has the same sign of the net signed area along the tube over one cycle, which implies that the sign of a net flow can be explained by the sign of net power; the larger net flow has the larger magnitude of the net signed area, which implies that the magnitude of a net flow can be explained by the amount of net power that is work done on the fluid by the fluid pressure and the elastic wall over one period: the rate of energy change along the tube over one period. A detailed description of the fluid dynamics in the three-dimensional model and the model of an open elastic tube in a tank and its related numerical results will be discussed in the separate papers.

Acknowledgements

We are indebted to Charles Peskin, David McQueen and Estarose Wolfson for the use of their visualization software and also for their technical assistance. We thank Do Wan Kim, Joonhyun Yeo, and Yongsam Kim for useful discussions. Jung's work was supported by Korea Research Foundation Grant (KRF-2004-015-C00063) and Lim's work was supported in part by the National Science Foundation under agreement No.0112050 at the Mathematical Biosciences Institute of Ohio State University, where Lim was a postdoctoral fellow, and in part by the University of Cincinnati.

References

[1] C. Beattie, A.D. Guerci, T. Hall, A.M. Borkon, W. Baumgartner, R.S. Stuart, J. Peters, H. Halperin, J.L. Robotham, Mechanisms of blood flow during pneumatic vest cardiopulmonary resuscitation, J. Appl. Physiol. 70 (1991) 454–465.
[2] J.M. Criley, J.T. Niemann, J.P. Rosborough, S. Ung, J. Suzuki, The heart is a conduit in CPR, Crit. Care Med. 9 (1981) 373.
[3] T. Haas, W.G. Voelckel, V. Wenzel, H. Antretter, A. Desslc, K.H. Lindner, Revisiting the cardiac versus thoracic pump mechanism during cardiopulmonary resuscitation, Resuscitation 58 (1) (2003) 113–116.
[4] H.R. Halperin, J.E. Tsitlik, R. Beyar, N. Chandra, A.D. Guerci, Intrathoracic pressure fluctuations move blood during CPR: comparison of hemodynamic data with predictions from a mathematical model, Ann. Biomed. Engrg. 15 (1987) 85–403.
[5] A.I. Hickerson, D. Rinderknecht, M. Gharib, Experimental study of the behavior of a valveless impedance pump, Exp. Fluids 38 (4) (2005) 534–540.
[6] E. Jung, 2-D simulations of valveless pumping using the immersed boundary method, Ph.D. Thesis, Courant Institute, New York University, 1999.
[7] E. Jung, C.S. Peskin, Two-dimensional simulations of valveless pumping using the immersed boundary method, SIAM J. Sci. Comput. 23 (2001) 19–45.
[8] E. Jung, A mathematical model of valveless pumping: a Lumped model with time-dependent compliance, resistance, and inertia, Bull. Math. Biol. 69 (7) (2007) 2181–2198.
[9] G. Liebau, Die Bedeutung der Tragheitskrafte fur die Dynamik des Blutkreislaufs, Z. Kreislaufforsch. 46 (1957) 428–438.
[10] G. Liebau, Die Stromungsprinzipien des Herzens, Z. Kreislaufforsch. 44 (1955) 677–684.
[11] G. Liebau, Uber ein Ventilloses Pumpprinzip, Naturwissenschsften 41 (1954) 327–328.
[12] G. Liebau, Ursache and Wirkung des hohen Druckgefälles im Arteriolenbereich, Z. Kreislaufforsch. 47 (1958) 385.
[13] G. Liebau, Beobachtungen über ventillose Förderung im Kapillargewebe Kreislauf, Verh. Dtsch. Ges. Kreislaufforsch. 29 (1963) 152.
[14] S. Lim, C.S. Peskin, Simulations of the whirling instability by the immersed boundary method, SIAM J. Sci. Comput. 25 (2004) 2066–2083.

[15] C.G. Manopoulos, D.S. Mathioulakis, S.G. Tsangaris, One-dimensional model of valveless pumping in a closed loop and a numerical solution, Phys. Fluids 18 (2006) 017106.
[16] A.M. Messner, A surface integral method for computer calculation of mass properties, SAWE Paper 852, in: Proceedings from 29th Annual Conference of the SAWE, Washington, DC, May 1970.
[17] A.M. Messner, G.Q. Taylor, Algorithm 550, solid polyhedron measures [Z], ACM Trans. Math. Software 6 (1) (1980) 121–130.
[18] K.L. Moore, Embryologie, Lehrbuch and Atlas der Entwicklungsgeschichte des Mens, second ed., Schattauer, Stuttgart, 1985, pp. 340–358.
[19] M. Moser, J.W. Huang, G.S. Schwarz, T. Kenner, A. Noordergraaf, Impedance defined flow, generalisation of William Harvey's concept of the circulation – 370 years later, Int. J. Cardiovasc. Med. Sci. 71 (1998) 205–211.
[20] J.T. Ottesen, Valveless pumping in a fluid-filled closed elastic tube-system: one-dimensional theory with experimental validation, J. Math. Biol. 46 (2003) 309–332.
[21] C.S. Peskin, D.M. McQueen, Fluid dynamics of the heart and its valves, in: H.G. Othmer, F.R. Adler, M.A. Lewis, J.C. Dallon (Eds.), Case Studies in Mathematical Modeling: Ecology, Physiology, and Cell Biology, Prentice-Hall, Englewood Cliffs, NJ, 1996, pp. 309–337.
[22] D. Rinderknecht, A.I. Hickerson, M. Gharib, A valveless micro impedance pump driven by electromagnetic actuation, J. Micromech. Microengrg. 15 (2005) 861–866.
[23] H. Thomann, A simple pumping mechanism in a valveless tube, J. Appl. Math. Phys. 29 (1978) 169–177.
[24] L. Zhu, C.S. Peskin, Simulation of a flapping flexible filament in a flowing soap film by the immersed boundary method, J. Comput. Phys. 179 (2002) 452–468.